Polaron formation as the vertex function problem: From Dyck's paths to self-energy Feynman diagrams

Tomislav Miškić[1*] **Juraj Krsnik**[1] **Andrey S. Mishchenko**[1,2] **and Osor S. Barišić**[1]

1 Department for Research of Materials under Extreme Conditions, Institute of Physics, HR-10000 Zagreb, Croatia
2 RIKEN Center for Emergent Matter Science (CEMS), Wako, Saitama 351-0198, Japan

⋆ tmiskic@ifs.hr

Abstract

We present a novel iterative method for generating all self-energy Feynman diagrams of any given order for the single polaron problem. This approach offers an effective tool for circumventing the sign problem that often arises in approximation-free numerical summations of Feynman diagrams. Each iterative step begins by rigorously listing all noncrossing diagrams using the graphical Dyck path representation of Stieltjes-Rogers polynomials, which exactly encode the Feynman diagram series. In the second phase, the Ward-Takahashi identity is used to uniquely identify the complete subset of vertex function contributions from the self-energy diagrams obtained in the previous iterative step. Finally, the noncrossing diagrams and vertex function contributions are combined to construct the full set of Feynman diagrams at a given order of the diagrammatic expansion, determining the number of diagrams of various types. This approach establishes a systematic procedure for generating the total sum of diagrams in a given order, enabling significant sign cancellation and making it broadly suitable for numerical summation techniques involving Feynman diagrams.

1   Introduction

The power of Feynman's diagram technique rests on its ability to formulate the perturbation series order by order rigorously and eventually sum up the series without approximations or extrapolate it to infinite order to obtain the exact answer [1]. Purely analytical methods can only reach the exact solution for a limited number of problems [1], and the contemporary trend is to sum up the series using numerical techniques. One of the most successful approaches is the Diagrammatic Monte Carlo (DMC), where the Metropolis protocol is used to perform a random walk between different orders and topologies of Feynman diagrams, leading to unbiased results for the Green or some other correlation function [2, 3].

In particular, the diagrammatic Monte Carlo (DMC) technique successfully solved some models of a single polaron [4–7]. However, the strategy of a random walk between different orders and topologies of Feynman diagrams is ineffective for the series of signs alternating diagrams as, for example, happens [8] for Barišić-Labbe-Friedel-Su-Schrieffer-Heeger (BLF-SSH) model [9–12] and many other models where the elements of the electron-phonon or other interaction matrix depend both on the phonon and the electron momenta [13, 14]. The general remedy for a problem with sign-alternating series was found for the first time in relation to the fermion sign problem, the most severe sign problem in the Feynman diagrammatic technique. The idea, circumventing the problem of alternating signs of the same order individual diagrams of different topologies, is to combine all diagrams of the same order into a single object where massive cancellations of signs result in sign definite object [15]. The object of order n consists of a sum of all diagrams with n-vertices (each having an interaction line and the in- and out-going Green function of fermions) connected in all possible ways. The object can then be fully determined by imaginary times (or Matsubara frequencies) and momenta (or positions in direct space) of the vertices.

The solution of the many-fermion sign problem implies a rather time-consuming procedure of recursive subtraction of nonconnected diagrams of determinant expansion [16, 17]. However, the perturbation expansion for the single polaron problem is simpler because the Feynman diagrams, in this case, are restricted to those where the fermion Green function propagates only forward in real/imaginary time and the phonon Green function is unrenormalized. Therefore, one can search for less complicated methods to create objects for the DMC with a cured sign problem than those used in many-fermion problems.

In this paper, we present an algorithm for systematically generating all Feynman diagrams of a given order for the polaron problem. The method constructs all possible diagram topologies by combining noncrossing and vertex function diagrams. This enables the construction of composite objects that include all diagrams in a given order, leading to significant cancellation
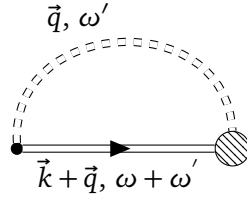
Figure 1: Diagrammatic representation of the exact electron irreducible self-energy in terms of the exact electron/hole propagator given by the double solid line, the exact phonon propagator given by the double dashed line, the bare and the exact vertex, given by the full black circle and the shaded blob, respectively.

of sign fluctuations between individual topologies. It also provides an effective tool for determining the number and types of Feynman diagrams in each order. Although we illustrate the method with a few explicit expressions from the Holstein model within the zero-temperature formalism, the approach itself is general, reflecting the universal diagrammatic structure of the polaron problem.

In Section 2 we express the exact self-energy and its value in self-consistent Born-Oppenheimer (SCBO) approximation in terms of continued fractions. In Section 3 we expand the continued fractions in terms of Stieltjes-Rogers polynomials, demonstrate the graphical representation of the polynomials in terms of Dyck paths, and show that there is a bijection between the Dyck paths and the SCBO diagrams. In Section 4 we perform a polynomial expansion of the exact self-energy and show that the expansion lists all possible Feynman diagrams of the given order. In Section 5 we use the Ward-Takahashi identity and show how to generate all vertex function contributions of the given order n from the self-energy diagrams of the same order n. Section 6 contains an algorithm to generate all self-energy Feynman diagrams from the Dyck paths, together with our results for counting the number of different Feynman diagrams of different types. Section 7 presents our conclusions.

2 Polaron problem

2.1 Exact electron self-energy in the polaron limit

The exact irreducible electron self-energy for the electron-phonon coupled system $\underline{\Sigma}_k(\omega)$ is shown in Fig. 1. It involves the double solid line representing the exact electron/hole propagator, $\underline{G}_k(\omega)$, and the exact phonon propagator, $\underline{D}_q(\omega)$, represented by the double dashed line. The bare, $g_{k+q,q}$, and the exact vertex, $g_{k+q,q}\underline{\Gamma}_{k+q,k}(\omega + E, \omega)$ (with $\underline{\Gamma}$ being the exact vertex function), are represented by the full black circle and the shaded blob, respectively. The self-energy may be expressed in the integral form [18],

$$\underline{\Sigma}_k^{n_e}(\omega) = \frac{i}{N} \sum_q |g_{k+q,q}|^2 \int \frac{d\omega'}{2\pi} \underline{G}_{k+q}(\omega + \omega')\underline{D}_q(\omega')\underline{\Gamma}_{k+q,k}(\omega + \omega', \omega) , \qquad (1)$$

where n_e denotes the density of permanent electrons in the system. The propagators $\underline{G}_k(\omega)$ and $\underline{D}_q(\omega)$ in Eq. (1) involve infinite series of reducible diagrams. Furthermore, while there is only one skeleton diagram associated with the exact self-energy $\underline{\Sigma}_k(\omega)$, the exact vertex involves an infinite series of such diagrams [19]. Thus, the evaluation of Eq. (1) represents a formidable task, and any simplification or approximation that is justified for some regimes of parameters is a matter of interest [20–24].

Figure 2: Diagrammatic content of Eq. (5) for the exact electron self-energy. Each self-energy insertion $\underline{\Sigma}_{k+q}(\omega - \omega_q)$ involves an exact electron propagator $\underline{G}_{k+q}(\omega - \omega_q)$, represented by a double line and contributed by all reducible self-energy diagrams. Each self-energy insertion $\underline{\Sigma}_{k+q}(\omega - \omega_q)$, according to Fig. 1 and Eq. (4), includes one bare and one exact vertex.

In the diagrammatic expansion of the exact self-energy $\underline{\Sigma}_k^{n_e}(\omega)$, the arguments of all phonon propagators are internal variables, q and ω', over which the summation/integration should be performed. The polaron problem corresponds in Eq. (1) to an electron excitation intermittently added to an otherwise empty band, i.e., $n_e = 0$. In this case, within the zero-temperature formalism considered explicitly throughout this paper, the propagator $\underline{G}_k(\omega)$ in Eq. (1) represents an electron in the state k propagating forward in time only, with all the poles of $\underline{G}_k(\omega)$, $\underline{\Sigma}_k(\omega)$, and $\underline{\Gamma}_{k+q,k}(\omega + \omega', \omega)$, appearing in the lower complex half-plane of ω. On the other hand, the exact phonon propagator remains unrenormalized since it corresponds to a system with no electrons,

$$
\underline{D}_q(\omega) \to D_q(\omega) = \frac{1}{\omega - \omega_q + i\eta} - \frac{1}{\omega + \omega_q - i\eta} \, , \tag{2}
$$

with $D_q(\omega)$ denoting the bare phonon propagator. With no hole excitations in the system, the integration over internal frequency ω' in Eq. (1) is contributed by the second term in Eq. (2), corresponding to the only pole that is found in the upper complex half-plane of ω' in Eq. (1),

$$
\underline{\Sigma}_k(\omega) = \sum_q \frac{|g_{k+q,q}|^2}{N} \underline{G}_{k+q}(\omega - \omega_q)\underline{\Gamma}_{k+q,k}(\omega - \omega_q, \omega) \, . \tag{3}
$$

By substituting $\underline{G}_{k+q}(\omega - \omega_q)$ in Eq. (3) using the Dyson equation,

$$
\underline{G}_k(\omega) = \frac{1}{G_k^{-1}(\omega) - \underline{\Sigma}_k(\omega)} \, , \tag{4}
$$

the self-energy can formally be rewritten in terms of itself. By recursively repeating this substitution procedure, i.e., each time replacing the exact electron propagator within the self-energy with its own Dyson expansion, the self-energy ultimately takes the form of an infinite continued fraction,

$$
\underline{\Sigma}_k(\omega) = \frac{1}{N}\sum_q \frac{|g_{k+q,q}|^2 \underline{\Gamma}_{k+q,k}(\omega - \omega_q, \omega)}{G_{k+q}^{-1}(\omega - \omega_q) - \frac{1}{N}\sum_{q'} \dfrac{|g_{k+q+q',k+q}|^2 \underline{\Gamma}_{k+q+q',k+q}(\omega - \omega_q - \omega_{q'}, \omega - \omega_q)}{G_{k+q+q'}^{-1}(\omega - \omega_q - \omega_{q'}) - \dots}} \, , \tag{5}
$$

where $G_k(\omega)$ is the bare electron propagator,

$$G_k(\omega) = \frac{1}{\omega - \varepsilon_k + i\eta} \, , \tag{6}$$

with ε_k the electron dispersion. This way of expressing the exact self-energy $\underline{\Sigma}_k(\omega)$ seems to be absent in the literature. It follows from Eq. (5) that the polaron problem is, in essence, a problem of finding the exact vertex function $\underline{\Gamma}_{k,k'}(\omega, \omega')$. Furthermore, in Eq. (5), the summation over momenta q may be generalized to involve a summation over different phonon branches. That is, Eq. (5) is the general equation relating the exact self-energy and the exact vertex function with a single electron characterized by dispersion ε_k, being linearly coupled to lattice phonons [25–30] (or any bosons [31–34]) with dispersion ω_q.

The diagrammatic content of Eq. (5) is illustrated in Fig. 2. One observes that all self-energy diagrams may be represented in the form of noncrossing diagrams, with one of the two vertices in each self-energy insertion being the exact vertex and the other being the bare vertex. Thus, only the vertex function $\underline{\Gamma}$ involves processes in which the phonon lines may cross, while all other phonon lines remain non-crossing. The rightmost vertex in Fig. 2 corresponds to the exact vertex in Fig. 1. The other renormalized vertices in Fig. 2 are associated with the renormalization of the exact electron propagator in Eq. (3), corresponding to an infinite series of reducible self-energy diagrams: $\underline{G} = G + G\underline{\Sigma}G + G\underline{\Sigma}G\underline{\Sigma}G + \cdots$. Each self-energy insertion in Fig. 2 again contains the exact electron propagator, meaning that the standard diagrammatic expansion that follows from the Wick theorem precisely follows the structure of Fig. 2.

2.2 Local self-energy

While the problem of coupled electron-phonon systems demands particular attention on the momentum dependence of vertex corrections [35], a few important properties of the diagrammatic expansion are parameter-independent. In particular, the number and the topology of diagrams are the same for any electron-phonon model with linear coupling to the lattice, which permits an insight into the structure of diagrammatic expansion by considering the limit in which the exact self-energy is momentum-independent (local), $\underline{\Sigma}_k(\omega) \to \underline{\Sigma}(\omega)$.

In the broader context of polaron physics, there are a few important cases in which the exact self-energy is local. For the Holstein model with local electron-phonon coupling $g_{k,k+q} = g$ and nondispersive optical phonons $\omega_q = \omega_0$, the self-energy becomes local when the vertex corrections are neglected. According to Fig. 2, the remaining diagrams are the noncrossing diagrams, corresponding to the self-consistent Born-Oppenheimer (SCBO) approximation. Indeed, for the Holstein model, setting $\underline{\Gamma} = 1$ in Eq. (5) gives

$$\Sigma_{SCBO}(\omega) = \cfrac{g^2 G_0(\omega - \omega_0)}{1 - \cfrac{g^2 G_0(\omega - \omega_0) G_0(\omega - 2\omega_0)}{1 - \cfrac{g^2 G_0(\omega - 2\omega_0) G_0(\omega - 3\omega_0)}{1 - \ldots}}} \, , \tag{7}$$

with $G_0(\omega) = \frac{1}{N}\sum_k G_k(\omega)$, being the bare local propagator, characterized solely by the dispersion of the noninteracting electrons. Thus, with momentum-independent coupling g, the SCBO self-energy has no k-dependence on any lattice geometry and dimension.

In the limit of nondispersive electrons (local limit), $\varepsilon_k \to \varepsilon_0$, the bare electron propagator in Eq. (6) becomes the same as the local propagator $G_0(\omega)$. In this limit, the exact solution of the Holstein polaron problem is given by [36]

$$\underline{\Sigma}_0(\omega) = \cfrac{g^2 G_0(\omega - \omega_0)}{1 - \cfrac{2g^2 G_0(\omega - \omega_0)G_0(\omega - 2\omega_0)}{1 - \cfrac{3g^2 G_0(\omega - 2\omega_0)G_0(\omega - 3\omega_0)}{1 - \dots}}} \ . \tag{8}$$

Furthermore, $\underline{\Sigma}_0(\omega)$ is the exact solution of the Holstein impurity problem as well [37], characterizing the interaction between the impurity and the electron. The exact self-energy is local in the limit of infinite dimension too. It may be obtained in the context of the Dynamical mean-field theory [36], which provides the exact solution by treating the impurity problem self-consistently. In this case, the local propagator in Eq. (8) physically represents the propagation of the electron entering and leaving the same lattice site m, $G_0(\omega) \rightarrow G_{m,m'}(\omega)\delta_{m,m'}$. Diagrammatically, $G_{m,m}(\omega)$ involves phonon excitations at other lattice sites as well ($m \neq m'$) [35], and should not be confused with the bare local propagator $G_0(\omega)$.

Comparing Eq. (7) and Eq. (8), it is easy to argue that the SCBO approximation offers a limited improvement over the approximation that considers the leading self-energy contribution only, highlighting the breakdown of the Migdal approximation. Namely, for sufficiently high densities of itinerant charges, characterized by a Fermi energy much larger than the phonon energies, $E_F \gg \omega_q$, the Migdal argument [38] of the unimportance of vertex corrections may be invoked into consideration. However, this argument does not apply to the polaron formation, which is a single-electron problem, $E_F \rightarrow 0$. We next consider, order-by-order, which diagrams appear in different orders of the diagrammatic expansions in Eqs. (7) and (8). Expansion of continued fractions in Eqs. (7) and (8) into an infinite series of Stieltjes-Rogers polynomials allows us to derive an algorithm constructing an order-by-order exact classification of the Feynman diagrams using the initial generation of its noncrossing subclass.

3 Dyck's paths and the SCBO diagrams

In this section we perform Stieltjes-Rogers polynomials expansion of SCBO continued fraction in Eq. (7) which allows us to formulate the robust and well-defined approach of generating the SCBO diagrams subclass, using a graphical representation of Dyck path. In particular, we show that the Dyck path approach considerably simplifies the generation of all topologically inequivalent irreducible noncrossing self-energy diagrams.

3.1 Stieltjes-Rogers polynomials

A remarkable property of the exact local self-energy in Eq. (8) in the local limit is that it incorporates all vertex correction contributions as simple numerical factors. To appreciate this, it suffices to compare Eq. (8) with the SCBO approximation in Eq. (7), which omits vertex corrections. In both cases, the self-energy takes the form of a continued fraction. We therefore turn our attention to a set of mathematical tools that prove particularly useful for diagrammatic expansions. In particular, we show that Eqs. (7) and (8) can be expressed as infinite series involving Stieltjes–Rogers polynomials [39–43]. From a physical perspective, this allows for a detailed analysis of the contributions from different classes of diagrams.

The general form of the Stieltjes continued fractions, abbreviated as $\mathcal{S}$-fractions, is given by [39],

$$S(\mathfrak{X},z) = \cfrac{c_0 \,|\, c_0 z^2}{1 - \cfrac{a_0 \,|\, b_1 z^2}{1 - \cfrac{a_1 \,|\, b_2 z^2}{1 - \ldots}}} = \frac{c_0 \,|\, c_0 z^2}{1 + \mathcal{K}_{r=0}^{+\infty}\left(-a_r \,|\, b_{r+1} z^2 : 1\right)}. \tag{9}$$

Here, $\mathcal{K}$ is used in a standard way to denote the continued fraction in a more compact form, while $\mathfrak{X}$ stands for a given set of coefficients a_i and b_i. The vertical bar $|$ means that the following denominator is inserted between the factors on the left and right sides during the expansion of the fraction. The $c_0^2 z^2$ factor is to account for the leading contribution in the expansion (in our case $c_0^2 z^2 = g^2 G_0 (\omega - \omega_0)$). The set of all Stieltjes-Rogers polynomials of all lengths will be represented by $\mathcal{P}$. The S-fraction corresponds to an infinite sum [39],

$$S(\mathfrak{X},z) = c_0^2 z^2 \cdot \sum_{k=0}^{+\infty} R_{2k}(\mathfrak{X}) \cdot z^{2k}, \tag{10}$$

where R_{2k} are the Stieltjes-Rogers polynomials. In the context of the diagrammatic expansion, it is apparent that z in Eq. (10) takes the role of the perturbative (coupling) parameter, with k defining the order n of perturbative expansion, $n = 2k + 2$. The Stieltjes-Rogers polynomials R_{2k} are given by $R_0(\mathfrak{X}) = 1$, and

$$R_{2k>0}(\mathfrak{X}) = \sum_{h=1}^{k-1} \sum_{\vec{m} \in \mathcal{A}_k^h} \left(\prod_{j=0}^{h-1} \binom{m_j + m_{j+1} - 1}{m_j - 1} \right) \left(\prod_{r=0}^{h} (a_r b_{r+1})^{m_j} \right), \tag{11}$$

where each set $\mathcal{A}_k^h$ of vectors $\vec{m}$, depending on k and h, is defined by two constrains for the components m_j of $\vec{m}$, given by [39]

$$\mathcal{A}_k^h = \left\{ \vec{m} \in \mathbb{N}_0^{h+1} : \left(\sum_{j=0}^{h} m_j = k \right) \wedge \left(m_h|_{h>1} \neq 0 \right) \right\}. \tag{12}$$

3.2 Graphical representation of Dyck paths

It is convenient to analyze the properties of the infinite series in Eq. (9), involving Stieltjes-Rogers polynomials, in terms of the Dyck paths [44, 45]. Namely, as established previously in the seminal paper by Flajolet [39], the Dyck paths represent combinatorial analogs of the S-fraction. In particular, each vector $\vec{m}$ in Eq. (12) corresponds to one of these paths.
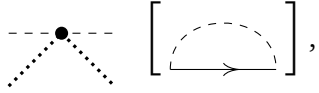
Graphically, the Dyck paths may be represented by discrete steps in the first quadrant of the $x - y$ plane, defined by the so-called "*up*" step, denoted here as a and equal to the vector $(1,1)$, and the "*down*" step, denoted as b and equal to the vector $(1,-1)$, such that they are below the diagonal of the first quadrant, beginning and ending at the same height $h = 0$. This implies that each path has an equal number of a and b elements, $n_a = n_b$, and that the height of a path in any given moment cannot be larger than the half-length of the path, $h \leq l/2$, where $l = n_a + n_b$. Therefore, to draw all Dyck paths of length l, $\mathcal{D}^{(l)}$, in our presentation, one has to draw all possible combinations of getting from point $(0,0)$ to $(l,0)$ using the elements a and b such that $0 \leq h \leq \frac{l}{2}$ always holds. Because of the non-commutativity of elements, we use a height index on every element as well, indicating not only the type of the step but also the height from which the step is taken.

Referring to Eq. (10), all Dyck paths may be expressed in terms of elements a, b, and c. In particular, each Dyck path corresponds to one element of the sets $\mathcal{A}_k^h$, defined by Eq. (12). If we are interested in all paths up to height h, we will truncate the fraction at the h-th denominator. For example, if we look at the first contribution in Eqs. (14)-(16), one may see
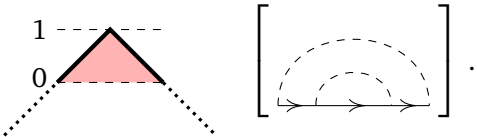
209 how it corresponds to the expansion of the fraction $\left(1 - a_0 b_1 g^2\right)^{-1}$ up to the first three terms.
210 Analogously, all other terms are obtained by expanding the higher-order fractions.
211   The Dyck path of length zero is given by
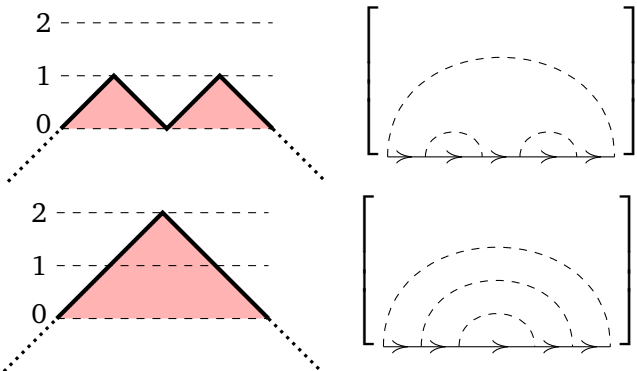
$$c_0^2 \equiv \quad 0 \text{ - - -} \bullet \text{ - - -} \quad \left[\; \overset{\frown}{\underset{\longrightarrow}{\quad}} \; \right], \tag{13}$$

212 and is depicted as a dot with zero height. Here, the dotted line represents the factor c_0. For
213 later purposes, together with the Dyck paths, we show the corresponding SCBO diagrams in
214 the square brackets. In particular, one may see that the factor c_0 represents a constant shift of
215 the Dyck path height by the value of one so that its height faithfully represents the number of
216 phonons in the system at a given time, $n_{ph} = h + 1$.
217   Going further, the Dyck path of length two may be represented by a string $a_0 b_1$. In other
218 words, we take an "*up*" step from height zero, and then a "*down*" step from height one,

$$c_0 a_0 b_1 c_0 \equiv \quad \begin{matrix} 1 \\ 0 \end{matrix} \quad \left[\; \overset{\frown}{\underset{\longrightarrow}{\quad}} \; \right]. \tag{14}$$

219 Considering all Dyck paths of length four, we have two contributions,

$$\tag{15}$$

220 Finally, considering all paths of length six, one finds five Dyck paths in Eq. (16). For length
221 six, for the first time, we encounter two different Dyck paths with the same contribution, i.e.,
222 the second and the third in Eq. (16). Of course, with increasing length of Dyck paths, more
223 paths that have the same contribution appear.
224   The SCBO diagrams, corresponding to Fig. 2 with all the vertices being bare, are diagrams
225 without temporal crossing (intersecting) of phonon lines. For the polaron problem, each SCBO
226 Feynman diagram counts the cardinality of phonons in the system at any given moment. Since
227 the former holds, and, considering that every self-energy diagram starts and ends with the
228 same number of phonons, we can reach the important conclusion that there is an equivalence
229 between each SCBO Feynman diagram and each Dyck path. In other words, there is a bijection
230 between the Dyck paths and the SCBO diagrams, and it is very easy to draw diagrams from
231 the paths and vice versa, as exhibited explicitly in Eqs. (13-16).

$$c_0 a_0 \cdot (b_1 a_0 b_1 a_0 + b_1 a_0 a_1 b_2 + a_1 b_2 b_1 a_0 + a_1 b_2 a_1 b_2 + a_1 a_2 b_3 b_2) \cdot b_1 c_0$$

$$\tag{16}$$

In particular, to obtain an SCBO diagram from a Dyck path, one should do the following: (1) draw a fermion line with two *external* vertices, (2) introduce l *internal* vertices between two *external* vertices where l represent the length of the Dyck path, (3) going from left to right, for every *up/down* step of the Dyck path create/annihilate a phonon line at the leftmost free *internal* vertex avoiding the crossing of any two phonon lines, (4) connect the two *external* vertices with a phonon line. With this, for example, it is easy to see that the Dyck paths of maximal height, $h = l/2$, correspond to rainbow diagrams.

4 Polynomial expansion of the exact self-energy

Using Stieltjes-Rogers polynomials, the SCBO self-energy in Eq. (7), as well as the exact self-energy in Eq. (8), may be easily expressed in a polynomial form. In particular, recognizing Eq. (8) as the $\mathcal{S}$-fraction defined by Eq. (9), with $z^2 = g^2$, $c_0^2 z^2 = g^2 G_0(\omega - \omega_0)$, and the set $\mathfrak{X}$ of coefficients given by

$$a_r = G_0(\omega - (r+1)\omega_0)$$

$$b_r = (r+1)G_0(\omega - (r+1)\omega_0),$$ (17)

Eq. (8) may be written as an infinite series,

$$\underline{\Sigma}(\omega) = g^2 G(\omega - \omega_0)\mathcal{S}(\mathfrak{X}, g^2) = g^2 G(\omega - \omega_0)\sum_{k=0}^{+\infty} R_{2k}(\mathfrak{X}) g^{2k},$$ (18)

where the Stieltjes-Rogers polynomial of order $2k > 0$, R_{2k}, is given by Eq. (11). Thus, the self-energy leading order contribution is given by

$$\Sigma^{(2)}(\omega) = g^2 G(\omega - \omega_0),$$ (19)

while, for the higher-order $n = 2k + 2$ contributions, one gets

$$\begin{aligned}
\underline{\Sigma}^{(n)}(\omega) &= g^n G(\omega - \omega_0)\sum_{h=1}^{n/2-1}\sum_{\vec{m}\in\mathcal{A}_{n/2}^h}\left(\prod_{j=0}^{h-1}\binom{m_j + m_{j+1} - 1}{m_j - 1}\right) \\
&\times \left(\prod_{r=0}^{h}(r+2)^{m_j}G^{m_j}(\omega - (r+1)\omega_0)G^{m_j}(\omega - (r+2)\omega_0)\right).
\end{aligned}$$ (20)

The sets $\mathcal{A}_{n/2}^h$ are defined by Eq. (12). In the SCBO case, b_r in Eq. (17) just needs to be replaced by $b_r = G_0(\omega - (r+1)\omega_0)$.

Each contribution $\underline{\Sigma}^{(n)}(\omega)$ in Eq. (20) corresponds to all the irreducible self-energy Feynman diagrams for a given order of perturbation theory. The same kind of derivation may be used to express the exact electron propagator $\underline{G}(\omega)$ in terms of Stieltjes-Rogers polynomials as well. The difference is that in the latter case, the diagrammatic expansion involves all the self-energy diagrams, reducible and irreducible.

4.1 Low-order vertex corrections

Using Eq. (20), the 4-th order contributions to the exact self-energy in Eq. (8) are obtained in the following form,

$$\Sigma^{(4)}(\omega, u \in \mathcal{P} \cap \mathfrak{X}_1^*) = \delta_{u, a_0 b_1} \cdot 2g^4 G_0^2(\omega - \omega_0)G_0(\omega - 2\omega_0)$$ (21)

$$\Sigma^{(4)}(\omega, a_0 b_1) \equiv \quad \text{(diagram)} \quad + \quad \text{(diagram)} \quad .$$ (22)

$\mathfrak{X}_i^*$ denotes all different strings of all lengths that include all a coefficients up to a_{i-1} and all b coefficients up to b_i, given by Eq. (17). The phonon and electron propagators highlighted in red correspond to the leading diagrammatic contribution to the exact vertex function in Fig. 1. In the case of the exact local self-energy in Eq. (8), the two diagrams in Eq. (22) contribute identically, resulting in the factor of 2 in Eq. (21). Similar combinatorial factors appear at higher orders, reflecting the number of distinct Feynman diagrams that yield the same contribution.

Following Eq. (20), the diagrammatic contributions corresponding to the sixth order of perturbation theory are given by

$$\Sigma^{(6)}\left(\omega, u \in \mathcal{P} \cap \mathfrak{X}_2^*\right) = \delta_{u, a_0^2 b_1^2} \cdot 4g^6 \, G_0^3(\omega - \omega_0)G_0^2(\omega - 2\omega_0)$$
$$+ \delta_{u, a_0 a_1 b_1 b_2} \cdot 6g^6 \, G_0^2(\omega - \omega_0)G_0^2(\omega - 2\omega_0)G_0(\omega - 3\omega_0) \tag{23}$$

269

(24)

270

(25)

271 Again, the parts of the diagrams corresponding to the exact vertex part of the diagram in Fig. 1
272 are highlighted in red, while the vertex correction that contributes to the exact Green function
273 is in blue. Just as in the fourth order, the sum of the prefactors of different products of free
274 propagators corresponds to the total number of irreducible self-energy diagrams.

275   In the eighth order, there are too many contributions to sketch them all here, so we will
276 only sketch the SCBO analogs of Dyck paths of length eight,

(26)

All other irreducible contributions with the vertex corrections, derived from the given Dyck path, may be obtained by specific permutations of the phonon lines in the SCBO self-energy diagram. In particular, to generate graphically all irreducible contributions to the self-energy for the polaron problem from a given SCBO diagram, one must perform all permutations of temporally retarded phonon line vertices such that after permutation, the vertices that were temporally retarded remain temporally retarded relative to their temporally advanced counterparts. However, using Eq. (5) and Fig. 2, there is an alternative, much simpler way to generate all the irreducible self-energy diagrams with vertex corrections. As an intermediate step in deriving this alternative procedure, we investigate the properties of the exact vertex function first.

5 Closed-form expressions for the exact vertex function

Since according to Eq. (5) the polaron problem is basically the vertex function problem, we explore the local limit further to provide a prescription for generating all the diagrammatic contributions to the vertex function correctly. In general, when the self-energy is momentum-dependent, the Ward-Takahashi identity relates the vertex function to the self-energy in the long-wave limit only [1, 46, 47]. However, when the self-energy and the bare propagator are local, this identity applies for all momenta equally, which, for the polaron problem, permits a polynomial expression of the exact vertex function. In particular, the diagrammatic contributions to the vertex function appearing in any order of diagrammatic expansion of the electron self-energy may be obtained from the self-energy diagrams obtained in the previous lower order.

5.1 Exact self-energy and the Ward-Takahashi identity

For nondispersive phonons, $\omega_q = \omega_0$, the vertex function may be treated as a function of a single variable, ω. Specifically, with respect to frequency dependence, it suffices to know $\Gamma(\omega - \omega_0, \omega)$ to evaluate the continued fraction in Eq. (5). In the local limit, the exact vertex takes on a particularly simple form. By examining the diagram in Fig. 1, one finds that the exact self-energy in Eq. (8) is given by

$$\underline{\Sigma}(\omega) = g^2 \cdot \underline{G}(\omega - \omega_0) \underline{\Gamma}(\omega - \omega_0, \omega) \, , \tag{27}$$

or,

$$\underline{\Gamma}(\omega - \omega_0, \omega) = g^{-2} \underline{\Sigma}(\omega) \cdot \left(G^{-1}(\omega - \omega_0) - \underline{\Sigma}(\omega - \omega_0) \right) . \tag{28}$$

Thus, by knowing the exact self-energy, one immediately knows the vertex function. Furthermore, this property has to hold order-by-order in the diagrammatic expansion.

One may further use the exact local self-energy given by the Stieltjes-Rogers polynomials expression in Eq. (18) to expand the vertex function in powers of g^2,

$$
\begin{aligned}
\underline{\Gamma}(\omega - \omega_0, \omega) = 1 + \sum_{k=1}^{+\infty} g^{2k} \cdot &\left\{ R_{2k}(\omega) - G_0(\omega - \omega_0) G_0(\omega - 2\omega_0) R_{2k-2}(\omega - \omega_0) \right\} \\
&- G_0(\omega - \omega_0) G_0(\omega - 2\omega_0) \cdot \sum_{k,m=1}^{+\infty} g^{2k+2m} \cdot R_{2k}(\omega) R_{2m-2}(\omega - \omega_0) \, .
\end{aligned}
\tag{29}
$$

Alternatively, the exact vertex in Eq. (27) may be obtained following the Ward-Takahashi identity,

$$\underline{\Gamma}(\omega - \omega_0, \omega) = 1 + \frac{1}{\omega_0}\big(\underline{\Sigma}(\omega - \omega_0) - \underline{\Sigma}(\omega)\big). \tag{30}$$

or, in the polynomial form,

$$\underline{\Gamma}(\omega - \omega_0, \omega) = 1 + \frac{g^2}{\omega_0}\sum_{k=0}^{+\infty} g^{2k}\Big\{G_0(\omega - 2\cdot\omega_0)R_{2k}(\omega - \omega_0) - G_0(\omega - \omega_0)R_{2k}(\omega)\Big\}. \tag{31}$$

5.2 Diagrammatic representation of the vertex function

Due to the Ward-Takahashi identity in Eq. (30), on any given order of perturbation theory, the vertex function corrections $\Gamma^{(n)}$ may be obtained from the self-energy contributions $\Sigma^{(n)}$. That is, diagrammatically, any vertex function correction may be generated by inserting the bare vertex along one of the bare electron propagators appearing in the self-energy diagram, drawing the phonon line to the left/right from this additional vertex. This way of obtaining the vertex function diagrammatically has been noted in the literature [48]. Here, this is proven using the mathematical identity derived in Appendix A,

$$\prod_{n=1}^{l}\frac{1}{(\omega - \omega_n - \omega')} - \prod_{n=1}^{l}\frac{1}{(\omega - \omega_n)} =$$
$$\sum_{i=1}^{l}\frac{\omega'}{(\prod_{n<i}(\omega - \omega_n))(\omega - \omega_i)(\omega - \omega_i - \omega')\prod_{n'>i}(\omega - \omega_{n'} - \omega')}. \tag{32}$$

The left-hand side (LHS) of Eq. (32) reflects the structure of the Ward-Takahashi identity on the right-hand side (RHS) of Eq. (30), involving a general form of the self-energy given by a product of poles. Frequencies ω_n characterize the bare electron propagators shifted by phonon excitation energies, $\omega_n = \varepsilon_k + \sum_q \omega_q$ as they appear in the self-energy diagrams. For the Holstein model $\omega_q = \omega_0$, as in Eq. (30). On the other hand, the RHS of Eq. (32) reflects the diagrammatic content of the vertex function. That is, by summing over i, one obtains all vertex function contributions corresponding to a given self-energy diagram that is represented by the LHS of Eq. (32). All bare electron propagators for $n < i$ remain unchanged, while all those for $n > i$ acquire a shift of ω'. Thus, the self-energy contribution is split into two parts, just as would happen by inserting the bare vertex with one additional phonon excitation propagating to the left/right from this additional vertex.

All vertex function corrections of a given order g^n are obtained by repeating this insertion for each electron propagator within all self-energy diagrams of order g^n. To get all the self-energy diagrams in the next order, it is sufficient to consider Fig. 2. That is, one needs to identify all SCBO diagrams up to g^{n+2} and insert the vertex function contributions of lower order in such a way that the total order of the resulting self-energy diagrams equals g^{n+2}.

As an illustration of how the vertex function corrections may be generated, we start from the leading self-energy diagram. In particular, there is just one vertex function correction that may be obtained by inserting the bare vertex,

$$\Gamma^{(2)}(\omega - \omega_0, \omega) \equiv \quad \text{} \quad . \tag{33}$$

The leading vertex function correction in the local limit is thus given by

$$\Gamma^{(2)}(\omega - \omega_0, \omega) = g^2 G_0(\omega - \omega_0) G_0(\omega - 2\omega_0) \ . \tag{34}$$

By closing the external phonon leg onto the incoming fermion leg, and by cutting the remaining external electron leg, one obtains the expression for the second self-energy diagram in Eq. (22) with the vertex correction,

$$g^4 G_0^2(\omega - \omega_0) G_0(\omega - 2\omega_0) = g^2 G_0(\omega - \omega_0) \cdot \Gamma^{(2)}(\omega - \omega_0, \omega) \ . \tag{35}$$

In the next order of the expansion, from the two self-energy diagrams in Eq. (22) one gets all the vertex function corrections in the fourth order,

$$\tag{36}$$

In the local limit, this gives

$$\begin{aligned}
\Gamma^{(4)}(\omega - \omega_0, \omega) = {}& 2g^4 \cdot G_0^2(\omega - \omega_0) G_0^2(\omega - 2\omega_0) \\
& + 4g^4 \cdot G_0(\omega - \omega_0) G_0^2(\omega - 2\omega_0) G_0(\omega - 3\omega_0) \quad .
\end{aligned} \tag{37}$$

From Eq. (22), one sees that the self-energy corrections, which were used to construct the vertex function corrections in Eq. (36), may already contain vertex corrections of the lower order. This illustrates order-by-order the diagrammatic content of the Ward-Takahashi identity in Eq. (27) as well. In particular, checking the vertex corrections in red in Eqs. (24) and (25) one recognizes all the contributions in Eqs. (33) and (36).

6   Generating Feynman diagrams from Dyck paths

Based on the considerations developed so far, we argue that all the Feynman diagrams appearing in the diagrammatic expansion of the self-energy may be obtained from the Dyck paths. The prescribed procedure is a recursive approach where, starting from the leading self-energy diagram, we climb one order at a time, generating all the other diagrammatic contributions to the vertex function and the self-energy in four steps, as schematically depicted in Fig. 3.

First step: For a given order of perturbative expansion n, $n \geq 2$, derive all the Dyck paths of length $n - 2$. From these paths, draw all the corresponding Feynman SCBO diagrams.

Second step: For all the SCBO diagrams obtained in previous lower orders, replace the bare vertices in the SCBO diagrams with diagrammatic contributions to the vertex, ensuring that the total order of the Feynman self-energy diagrams obtained in this way is n. The vertex function corrections have to be inserted according to Fig. 2, replacing the left or right bare vertices in self-energy insertions, but not both of them.
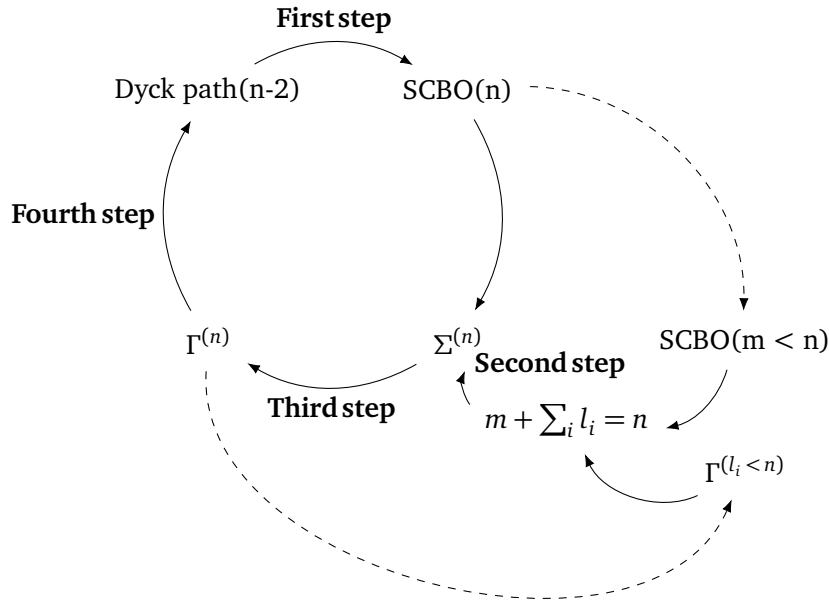
Figure 3: Scheme of the recursive procedure for the generation of self-energy Feynman diagrams from Dyck paths in four steps.

Third step: From all the self-energy diagrams obtained in the n-th order generate the diagrammatic contributions to the vertex function. All these contributions are obtained by inserting one bare vertex along each electron propagator in each self-energy diagram.

Fourth step: Return to the first step and repeat the procedure for the next order in the perturbative expansion $n + 2$.

In Table 1, we demonstrate how the prescribed procedure generates all Feynman diagrams up to order $n = 6$. Starting with $n = 2$, in the first step the above procedure gives the Dyck path of length zero and the corresponding lowest SCBO self-energy diagram. For $n = 2$, the second step does not apply and we may move to the third step, in which the leading vertex function correction, denoted in red, is obtained. Returning to the first step, for $n = 4$ the Dyck path of length two is obtained together with the corresponding SCBO diagram. Following now the prescription for the second step, the leading vertex function correction is inserted into the single $n = 2$ SCBO self-energy diagram, yielding the second irreducible self-energy diagram, with the inserted vertex correction similarly denoted in red and contributing to the vertex function in Fig. 1. Together with the single $n = 4$ SCBO diagram obtained in the first step, this reproduces the two existing 4th-order self-energy diagrams. In the third step, we generate all the 4th-order vertex function corrections from the 4th-order self-energy diagrams, which are now highlighted in blue. Continuing the procedure further for $n = 6$, for example, one may check that these blue vertex function correction diagrams, when inserted into the lowest $n = 2$ SCBO self-energy diagram, reproduce the six out of ten 6th-order self-energy diagrams, whose vertex correction parts to the vertex function are similarly denoted in blue. Two of the ten 6th-order self-energy diagrams are the SCBO diagrams corresponding to the two Dyck paths. As prescribed in the second step, the remaining two 6th-order self-energy diagrams are obtained by inserting the leading vertex function correction, denoted in red, into the single $n = 4$ SCBO diagram. One of these two vertex corrections contributes to the vertex function

in Fig. 1, whereas the second contributes to the exact propagator.

The described procedure is intriguing due to its combinatorial elegance and because it uses Dyck paths, whose cardinality is drastically smaller than the total number of self-energy diagrams. It provides a straightforward algorithm for generating all irreducible self-energy contributions for the polaron problem, which could accelerate and simplify computer algorithms for the generation of diagrammatic contributions.

	$\mathcal{D}^{(n-2)}$	$\Sigma_{SCBO}^{(n)}$	$\Sigma^{(n)}$	$\Gamma^{(n)}$
$n=2$				
$n=4$				
$n=6$				

Table 1: Order-by-order generation of the electron self-energy and vertex function corrections (highlighted in color) from Dyck paths. The vertex corrections contribute to both the exact electron propagator and the vertex function shown in Fig. 1.

6.1 Cardinality of diagrams

We now turn to the problem of counting the number of distinct diagrammatic contributions for the polaron problem. Specifically, we derive analytical expressions for the total number of self-energy diagrams and diagrammatic contributions to the vertex function corrections. These quantities are independent of any parameters and remain applicable regardless of the momentum dependence of the diagrams.

We approach the problem of counting all the self-energy diagrams, reducible and irreducible, in the n-th order of perturbation by gradually reducing it to simple problems until the trivial case is reached. We consider a set of n vertices in the n-th order of perturbation theory and find the number of different pairings of two points. The number of unordered samples without replacement of cardinality two of the set of n vertices is given by a 2-combination of the set of vertices. With every pair chosen, the cardinality of the set of vertices is subtracted by two, until we get down to only two vertices. Every step brings about the 2-combination factor equal to $\binom{2j-2i}{2}$, where i is the number of steps taken, so the total number of ways would be equal to the multiplication of said binomials,

$$\mathcal{I}_{tot}^{(n)} = \prod_{j=1}^{n/2} \frac{1}{j} \binom{2j}{2} \quad . \tag{38}$$

The above expression contains another factor equal to the inverse of the number of steps taken $\frac{1}{j}$. Using the associativity of multiplication on the real domain the factor $\frac{1}{j}$ becomes $\frac{1}{(n/2)!}$. The

factor $\frac{1}{(n/2)!}$ comes from the indistinguishability of phonon lines. Thus, for the total number of self-energy diagrams, one gets

$$\mathcal{I}_{tot}^{(n)} = (n-1)!! \, . \tag{39}$$

To address the problem of counting irreducible self-energy diagrams in the n-th order, we begin by observing that the prefactor in front of the propagator product specifies the number of diagrams generated by the algebraic expression. Therefore, to determine the total number of irreducible diagrams, it suffices to sum the prefactors in Eq. (20). Specifically, setting $a_i = 1$, and $b_i = i+1$, for each i, the expression for the number of irreducible diagrams in the $(n+2)$-th order is obtained,

$$\mathcal{I}_{irr}^{(n+2)}\big|_{n\geq 2} = \sum_{h=1}^{n/2-1} \sum_{\vec{i} \in \mathcal{A}_{n/2}^h} \left(\prod_{j=0}^{h-1} \binom{i_j + i_{j+1} - 1}{i_j - 1} \right) \cdot \left(\prod_{l=0}^{h} (l+2)^{i_l} \right), \tag{40}$$

where the sets $\mathcal{A}_{n/2}^h$ are those introduced in Eq. (12). The indexing $n + 2$ arises from the additional g^2 in Eqs. (18) and (20), so the $n/2$-th term in the summation in Eq. (18) counts the g^{n+2} contribution to the self-energy. Therefore, Eq. (40) gives an analytical expression for the number of irreducible self-energy corrections order by order of perturbation theory. That is, using Eq. (40), we may reproduce the known series 1, 2, 10, 74, 706, 8162... [49], which describes the number of irreducible corrections in each order of perturbation starting from $n = 2$, i.e., g^2 contribution. Now, it is easy to obtain the number of reducible diagrams by subtracting the number of all self-energy contributions and the cardinality of irreducible diagrams, $\mathcal{I}_{red}^{(n)} = \mathcal{I}_{tot}^{(n)} - \mathcal{I}_{irr}^{(n)}$.

The number of SCBO diagrams follows from the bijective mapping from the set of labeled Dyck paths to SCBO-approximated irreducible Feynman diagrams, established in Sec. 6. Therefore, by counting Dyck paths of length n, one obtains the irreducible SCBO contributions to the self-energy in the nth order as well. The number of Dyck paths is given by the famous Catalan sequence [50], so given the equivalence we write down the number of SCBO-approximated diagrams as,

$$\mathcal{I}_{\text{SCBO}}^{(n)} = C_{n/2} = \frac{1}{n/2+1} \binom{n}{n/2} \, . \tag{41}$$

As already shown, all the diagrammatic contributions to the vertex function may be generated by inspecting the self-energy diagrams of the same order and by inserting an additional phonon leg. The phonon leg has to be inserted into every free fermionic propagator. The self-energy contribution of the n-th order has $n-1$ free fermionic propagators. Thus, one just needs to multiply that by the number of irreducible diagrams to which we can insert the phonon leg.

$$\mathcal{I}_{ver.\ corr.}^{(n)} = (n-1) \cdot \mathcal{I}_{irr}^{(n)} \, . \tag{42}$$

Table 2 shows the cardinality of the SCBO diagrams, the cardinality of irreducible self-energy diagrams, and the cardinality of diagrammatic contributions to the vertex function. For comparison of growth rates, a factorial dependence is included as well. From Table 2 one sees that the number of SCBO-approximated diagrams, or the number of Dyck paths, grows very slowly compared to all the other quantities. Furthermore, we observe that the cardinality of diagrammatic contributions to the vertex function, which are the primary contributors to the complexity of the polaron problem, grows faster than $n/2!$. This highlights the critical role of vertex corrections in determining the computational difficulty of electron-phonon problems.

Order in coupling constant	g^2	g^4	g^6	g^8	g^{10}	g^{12}
Cardinality of SCBO diagrams	1	1	2	5	14	42
$(n/2)!$	1	2	6	24	120	720
Cardinality of irreducible $\underline{\Sigma}$ diagrams	1	2	10	74	706	8162
Cardinality of diagrammatic contributions to $\underline{\Gamma}$	1	6	50	518	6354	89782
Cardinality of diagrammatic contributions to $\underline{G}$	1	3	15	105	945	10395

Table 2: The comparison of the cardinality of Feynman diagrams in each order of perturbative expansion: number of SCBO approximated diagrammatic contributions, $n/2!$ growth, number of irreducible $\underline{\Sigma}$ diagrams, number of diagrammatic contributions to the vertex function, number of diagrammatic contributions to the exact Green function $\underline{G}$.

7 Conclusions

We have reduced the problem of polaron formation to that of determining the exact vertex function, deriving an expression for the electron self-energy in terms of a nested continued fraction involving the free electron propagator and the exact vertex function. Building on this insight, we developed a method to iteratively construct all self-energy diagrams by combining noncrossing and vertex correction diagrams obtained in previous iterative (lower-order) steps. Starting from the leading-order self-energy diagram, our simple four-step procedure (outlined in Section 6) generates higher-order diagrams systematically and straightforwardly. As a consistency check, we derived expressions to count the number of diagrammatic contributions to the exact vertex function, self-energy, and electron propagator at any order in the expansion.

To derive and establish the completeness of our method, we introduced Flajolet's combinatorial formalism of Stieltjes-type continued fractions into the physical setting of Feynman diagrammatics. Specifically, we expressed the exact self-energy as a continued fraction and represented it using Stieltjes-Rogers polynomials, which correspond graphically to the Dyck paths. We established a bijective mapping between the Dyck paths and the SCBO (noncrossing) Feynman diagrams. Using the expansion of the self-energy through Stieltjes-Rogers polynomials and invoking the Ward–Takahashi identity, we derived a corresponding expansion for the vertex function. This allowed us to prove a diagrammatic rule for constructing vertex function diagrams from self-energy diagrams of the same order, as a crucial step in generating all self-energy diagrams in the next order. We showed how vertex function corrections are systematically incorporated into SCBO self-energy diagrams to yield the full set of diagrams up to any desired order in the perturbative series.

Our method provides a particularly efficient way to navigate the complexity of high-order diagrammatic expansions, offering theoretical insights, as well as practical utility. In particular, it inherently accounts for all self-energy diagrams in a given order, thereby avoiding the alternating sign problem commonly encountered in diagrammatic techniques. Similar combinatorial techniques may be applied to a broader range of many-body problems, including those with finite electron densities and the renormalization of boson/interaction propagators.

Acknowledgements

Funding information   J.K., A.S.M., and O.S.B. acknowledge the support of the Croatian Science Foundation under the project numbers IP-2022-10-3382, IP-2024-05-2406, and IP-2022-10-9423, respectively. O.S.B. acknowledges the support of Project FrustKor financed by the EU through the National Recovery and Resilience Plan 2021-2026 (NRPP).

A Ward-Takahashi identity in terms of product of poles

We prove by induction that Eq. (32) holds for a product of any number of poles. First, we consider the base case $l = 1$, which can be shown to hold using a simple algebra,

$$\frac{1}{\omega - \omega_1 - \omega'} - \frac{1}{\omega - \omega_1} = \frac{\omega'}{(\omega - \omega_1)(\omega - \omega_1 - \omega')} . \tag{43}$$

Assuming that Eq. (32) holds for some $l \in \mathbb{N}$, it is sufficient to show now the same property for $l \to l + 1$. Starting with the RHS of Eq. (32), we derive the LHS of Eq. (32) for the case when the number of poles equals $l + 1$. Decomposing the summation for this case into a sum from 1 to l while treating the $(l + 1)$-th contribution separately, one gets

$$\sum_{i=1}^{l+1} \frac{\omega'}{(\prod_{n<i}(\omega - \omega_n))(\omega - \omega_i)(\omega - \omega_i - \omega')\prod_{n'>i}(\omega - \omega_{n'} - \omega')} = \frac{1}{\omega - \omega_{l+1} - \omega'} \cdot$$

$$\cdot \sum_{i=1}^{l} \frac{\omega'}{(\prod_{n<i}(\omega - \omega_n))(\omega - \omega_i)(\omega - \omega_i - \omega')\prod_{n'\in\langle i,l]_{\mathbb{N}}}(\omega - \omega_{n'} - \omega')} + \tag{44}$$

$$+ \frac{\omega'}{(\prod_{i=1}^{l}(\omega - \omega_i))(\omega - \omega_{l+1})(\omega - \omega_{l+1} - \omega')} .$$

Assuming that Eq. (32) holds for l, the RHS of Eq. (44) may be rewritten in the form given by

$$= \frac{1}{\omega - \omega_{l+1} - \omega'} \cdot \left(\frac{1}{\prod_{i=1}^{l}(\omega - \omega_i - \omega')} - \frac{1}{\prod_{i=1}^{l}(\omega - \omega_i)} \right) +$$

$$+ \frac{\omega'}{(\prod_{i=1}^{l}(\omega - \omega_i))(\omega - \omega_{l+1})(\omega - \omega_{l+1} - \omega')} , \tag{45}$$

which straightforwardly gives Eq. (32) for $l + 1$, completing the proof.

References

[1] G. D. Mahan, *Many Particle Physics*, Plenum Press, New York (1990).

[2] N. Prokof'ev, *Diagrammatic Monte Carlo*, Forschungszentrum Jülich, Jülich (2019).

[3] J. Greitemann and L. Pollet, *Lecture notes on Diagrammatic Monte Carlo for the Fröhlich polaron*, SciPost Phys. Lect. Notes p. 2 (2018), doi:10.21468/SciPostPhysLectNotes.2.

[4] N. V. Prokof'ev and B. V. Svistunov, *Polaron problem by diagrammatic quantum monte carlo*, Phys. Rev. Lett. **81**, 2514 (1998), doi:10.1103/PhysRevLett.81.2514.

[5] A. S. Mishchenko, N. V. Prokof'ev, A. Sakamoto and B. V. Svistunov, *Diagrammatic quantum monte carlo study of the fröhlich polaron*, Phys. Rev. B **62**, 6317 (2000), doi:10.1103/PhysRevB.62.6317.

[6] A. S. Mishchenko, N. Nagaosa, N. V. Prokof'ev, A. Sakamoto and B. V. Svistunov, *Self-trapping of polarons in the rashba-pekar model*, Phys. Rev. B **66**, 020301 (2002), doi:10.1103/PhysRevB.66.020301.

[7] A. S. Mishchenko and N. Nagaosa, *Quasidegenerate self-trapping in one-dimensional charge transfer exciton*, Phys. Rev. Lett. **86**, 4624 (2001), doi:10.1103/PhysRevLett.86.4624.

[8] D. J. J. Marchand, G. De Filippis, V. Cataudella, M. Berciu, N. Nagaosa, N. V. Prokof'ev, A. S. Mishchenko and P. C. E. Stamp, *Sharp transition for single polarons in the one-dimensional su-schrieffer-heeger model*, Phys. Rev. Lett. **105**, 266605 (2010), doi:10.1103/PhysRevLett.105.266605.

[9] S. Barišić, J. Labbé and J. Friedel, *Tight binding and transition-metal superconductivity*, Phys. Rev. Lett. **25**, 919 (1970), doi:10.1103/PhysRevLett.25.919.

[10] S. Barišić, *Rigid-atom electron-phonon coupling in the tight-binding approximation.i*, Phys. Rev. B **5**, 932 (1972), doi:10.1103/PhysRevB.5.932.

[11] S. Barišić, *Self-consistent electron-phonon coupling in the tight-binding approximation. ii*, Phys. Rev. B **5**, 941 (1972), doi:10.1103/PhysRevB.5.941.

[12] W. P. Su, J. R. Schrieffer and A. J. Heeger, *Solitons in polyacetylene*, Phys. Rev. Lett. **42**, 1698 (1979), doi:10.1103/PhysRevLett.42.1698.

[13] A. S. Mishchenko and N. Nagaosa, *Electron-phonon coupling and a polaron in the $t-j$ model: From the weak to the strong coupling regime*, Phys. Rev. Lett. **93**, 036402 (2004), doi:10.1103/PhysRevLett.93.036402.

[14] E. Burovski, H. Fehske and A. S. Mishchenko, *Exact treatment of exciton-polaron formation by diagrammatic monte carlo simulations*, Phys. Rev. Lett. **101**, 116403 (2008), doi:10.1103/PhysRevLett.101.116403.

[15] R. Rossi, *Determinant diagrammatic monte carlo algorithm in the thermodynamic limit*, Phys. Rev. Lett. **119**, 045701 (2017), doi:10.1103/PhysRevLett.119.045701.

[16] F. Šimkovic, R. Rossi and M. Ferrero, *Efficient one-loop-renormalized vertex expansions with connected determinant diagrammatic monte carlo*, Phys. Rev. B **102**, 195122 (2020), doi:10.1103/PhysRevB.102.195122.

[17] K. Van Houcke, F. Werner and R. Rossi, *High-precision numerical solution of the fermi polaron problem and large-order behavior of its diagrammatic series*, Phys. Rev. B **101**, 045134 (2020), doi:10.1103/PhysRevB.101.045134.

[18] I. E. D. A. A. Abrikosov, L. P. Gor'kov, *Methods of Quantum Field Theory in Statistical Physics*, Pergamon Press, Oxford (1965).

[19] A. L. Fetter and J. D. Walecka, *Quantum Theory of Many-Particle Systems*, McGraw-Hill, Boston (1971).

[20] V. V. Kabanov, *Adiabatic theory of the polaron spectral function*, J. Phys. Commun. **6**(115002) (2022), doi:ttps://doi.org/10.1088/2399-6528/ac9d81.

[21] O. S. Barišić and S. Barišić, *Quantum adiabatic polarons by translationally invariant perturbation theory*, The European Physical Journal B **54**(1), 1 (2006), doi:10.1140/epjb/e2006-00413-5.

[22] J. Loos, M. Hohenadler, A. Alvermann and H. Fehske, *Phonon spectral function of the holstein polaron*, Journal of Physics: Condensed Matter **18**(31), 7299 (2006), doi:10.1088/0953-8984/18/31/023.

[23] D. Dunn, *Electron–phonon interactions in an insulator*, Can. J. Phys. **53**(4), 321 (1975), doi:10.1139/p75-042.

[24] B. Gumhalter, V. Kovač, F. Caruso, H. Lambert and F. Giustino, *On the combined use of GW approximation and cumulant expansion in the calculations of quasiparticle spectra: The paradigm of si valence bands*, Phys. Rev. B **94**(3), 035103 (2016), doi:10.1103/physrevb.94.035103.

[25] H. Fröhlich, H. Pelzer and S. Zienau, *Xx. properties of slow electrons in polar materials*, The London, Edinburgh, and Dublin Philosophical Magazine and Journal of Science **41**(314), 221 (1950), doi:10.1080/14786445008521794.

[26] T. Holstein, *Studies of polaron motion*, Annals of Physics **8**(3), 325 (1959), doi:10.1016/0003-4916(59)90002-8.

[27] D. J. J. Marchand and M. Berciu, *Effect of dispersive optical phonons on the behavior of a holstein polaron*, Physical Review B **88**(6), 060301 (2013), doi:10.1103/PhysRevB.88.060301.

[28] J. Bonča, S. A. Trugman and M. Berciu, *Spectral function of the holstein polaron at finite temperature*, Physical Review B **100**(9), 094307 (2019), doi:10.1103/PhysRevB.100.094307.

[29] T. Hahn, N. Nagaosa, C. Franchini and A. S. Mishchenko, *Diagrammatic quantum monte carlo study of an acoustic lattice polaron*, Physical Review B **104**(16), l161111 (2021), doi:10.1103/PhysRevB.104.L161111.

[30] J. Bonča and S. A. Trugman, *Electron removal spectral function of a polaron coupled to dispersive optical phonons*, Physical Review B **106**(17), 174303 (2022), doi:10.1103/PhysRevB.106.174303.

[31] B. Bergersen, F. W. Kus and C. Blomberg, *Single particle green's function in the electron–plasmon approximation*, Canadian Journal of Physics **51**(1), 102 (1973), doi:10.1139/p73-012.

[32] F. Caruso and F. Giustino, *Theory of electron-plasmon coupling in semiconductors*, Physical Review B **94**(11), 115208 (2016), doi:https://doi.org/10.1103/PhysRevB.94.115208.

[33] S. Schmitt-Rink, C. M. Varma and A. E. Ruckenstein, *Spectral function of holes in a quantum antiferromagnet*, Physical Review Letters **60**(26), 2793 (1988), doi:10.1103/PhysRevLett.60.2793.

[34] P. Horsch and A. Ramšak, *Spin-polaron wave function for a single hole in an antiferromagnet*, Journal of Low Temperature Physics **95**(1–2), 343 (1994), doi:10.1007/bf00754950.

[35] O. S. Barišić, *Diagrammatic content of the dynamical mean-field theory for the holstein polaron problem in finite dimensions*, Phys. Rev. B **76**, 193106 (2007), doi:10.1103/PhysRevB.76.193106.

[36] S. Ciuchi, F. de Pasquale, S. Fratini and D. Feinberg, *Dynamical mean-field theory of the small polaron*, Phys. Rev. B **56**, 4494 (1997), doi:10.1103/PhysRevB.56.4494.

[37] J. Krsnik, I. Batistić, A. Marunović, E. Tutiš and O. S. Barišić, *Exact solution of electronic transport in semiconductors dominated by scattering on polaronic impurities*, Physical Review B **102**(24), 241111 (2020), doi:https://doi.org/10.1103/PhysRevB.102.241111.

[38] A. B. Migdal, *Interaction between electrons and lattice*, Sov. Phys. JETP **7**, 996 (1958).

[39] P. Flajolet, *Combinatorial aspects of continued fractions*, Discrete Mathematics **32**(2), 125 (1980), doi:https://doi.org/10.1016/0012-365X(80)90050-3.

[40] W. B. Jones and W. J. Thron, *Encyclopedia of mathematics and its applications: Continued fractions: Analytic theory and applications series number 11*, Cambridge University Press, Cambridge, England (2009).

[41] M. Pétréolle, A. Sokal and B.-X. Zhu, *Lattice paths and branched continued fractions: An infinite sequence of generalizations of the Stieltjes–Rogers and Thron–Rogers polynomials, with coefficientwise Hankel-total positivity*, vol. 291, American Mathematical Society (2023).

[42] D. Angell, *A family of continued fractions*, Journal of Number Theory **130**(4), 904 (2010), doi:https://doi.org/10.1016/j.jnt.2009.12.003.

[43] W. Van Assche, *The impact of stieltjes' work on continued fractions and orthogonal polynomials*, arXiv preprint math/9307220 (1993).

[44] D. F. Bailey, *Counting arrangements of 1's and -1's*, Mathematics Magazine **69**(2), 128 (1996).

[45] R. A. Brualdi, *Introductory combinatorics*, Pearson, Upper Saddle River, NJ, 5 edn. (2008).

[46] S. Engelsberg and J. R. Schrieffer, *Coupled electron-phonon system*, Physical Review **131**(3), 993 (1963), doi:10.1103/PhysRev.131.993.

[47] S. Pandey, *Ward identity preserving approach for investigation of phonon spectrum with self-energy and vertex corrections*, Physical Review B **110**(6), 064321 (2024), doi:10.1103/PhysRevB.110.064321.

[48] J. Bardeen, L. N. Cooper and J. R. Schrieffer, *Theory of superconductivity*, Phys. Rev. **108**, 1175 (1957), doi:10.1103/PhysRev.108.1175.

[49] G. L. Goodvin, M. Berciu and G. A. Sawatzky, *Green's function of the holstein polaron*, Phys. Rev. B **74**, 245104 (2006), doi:10.1103/PhysRevB.74.245104.

[50] R. P. Stanley, *Catalan Numbers*, Cambridge University Press (2015).